An Explainable Hierarchical Deep Representation Learning Framework for Multi-Class Host Rock Recognition from Mining Data

Sami F Karali[1], Mohammed I Thanoon[2], Majed Nawas[3], Ahlem Fatnassi[4], Abed Saif Ahmed Alghawli[5], Zakhriya Alhassan[6], Yahia Said[7]*

Computing Department-College of Engineering and Computing at Al-Lith, Umm Al-Qura University, Saudi Arabia[1, 2]
Department of Computer Science-College of Science, Northern Border University, Arar 73213, Saudi Arabia[3, 4]
Computer Science Department-College of Sciences and Humanities, Prince Sattam Bin Abdulaziz University, Aflaj 11912, Kingdom of Saudi Arabia[5]
College of Computer Science and Engineering, University of Jeddah, Jeddah, Kingdom of Saudi Arabia[6]
Center for Scientific Research and Entrepreneurship, Northern Border University, 73213, Arar, Saudi Arabia[7]

***Abstract*—This study aims to improve the automatic recognition of geological host rocks from mining data and to make the prediction process easier to understand for geologists, mining engineers, and data analysts. The study uses a mining dataset containing global mineral and rock information. The data are cleaned, missing values are handled, and the most useful features are selected through three feature selection methods. A deep learning model is then developed to learn hidden rock patterns, links among geological features, and differences between rock classes. The model combines several connected learning parts to capture local, regional, and broad geological patterns. A final classification step is used to identify different host rock types. Explanation tools are also applied to show which features most influence each prediction. The proposed model achieves strong results in recognizing several host rock classes, including limestone, andesite, diorite, gravel, granite, gneiss, sandstone, schist, quartzite, rhyolite, dolomite, alluvium, volcanic rock, and slate. The results show high accuracy in both training and testing data. The explanation results also help identify the geological features that contribute most to the model's decisions. The experimental evaluation is conducted using the Mineral Ores Around the World dataset to assess the effectiveness of the proposed framework for host rock classification. However, the proposed model achieved strong classification performance. Under the 80:20 training-testing split, it obtained an accuracy of 97.91%, and under the 70:30 split, it achieved an accuracy of 97.31%. The study offers an explainable deep learning framework that combines feature selection, multi-level pattern learning, and prediction explanation for host rock recognition. The approach can support faster geological interpretation, mineral exploration, mining planning, and decision-making, and may guide future work on explainable artificial intelligence for mining applications.**

Keywords*—Host rock recognition; mining data; feature selection; explainable artificial intelligence; geological feature selection; mineral exploration; multi-class rock recognition

I. Introduction

Recently, the field of mine geophysics has experienced significant growth in research focusing on enhancing the efficiency of exploration and mineral extraction. The increasingly complex geological conditions in modern mining industries require new innovative models for geophysical analysis [1]. The term host rock can refer to a part of the geosphere, particularly in a crystalline-basement setting where sedimentary cover is absent; it more often refers to a particular unit in the geosphere where the repository is situated [2]. In many situations, the host rock refers to the section of the geosphere that provides the most significant confinement for the waste, and it can be enclosed by units with less predictable or less favorable characteristics, including lithologically heterogeneous sequences or aquifers [3]. The classification of various rock units as subdivisions in the crystalline host rock is essential in determining the spatial distribution of significant chemical and physical characteristics in the rock mass [4]. Accurate observation of the neighboring rock deformation condition of mining roadways is important for building a smart coal mine system. During the tunneling process, the original equilibrium of the rock mass is disturbed, which may lead to a potential safety hazard of instability and damage in the neighboring rock [5].

Accurate categorization of multi-element geochemical information is a complex problem because complex geological features influence stream sediments' geochemical data [6]. The classification outcome of multi-element geochemical information can vary when different supervised learning methods are used [7]. Hence, choosing a suitable method for categorizing geochemical data tables into accurate classes of geochemical anomaly and background can reduce bias issues and uncertainty in geochemical anomaly mapping [8]. Thus, precise classification of geochemical samples is a challenging task in mineral exploration targeting. Over the past decades, various machine learning (ML) approaches have been used to classify geochemical data [9]. In this framework, supervised learning methods are used to categorize objects based on pre-defined labels, and unsupervised learning methods are applied to recognize hidden attributes of input without relying on pre-defined labels [10]. Shallow ML methods have a limited number of hidden layers and a lack of ability to capture deep representations from complex inputs [11]. Whereas deep learning methods have strong capabilities for handling complex data, which include various processing layers that capture high-level feature extraction [12].

A. Problem Statement and Research Contributions

Despite the improvements achieved in geological and geochemical data analysis, precise host rock classification still remains a challenging task owing to the intricate nature of mineral distributions, spatial geological dependencies, and heterogeneous mining data. Traditional machine learning methods often rely on shallow architectures and manual feature extraction, which may not efficiently capture multi-level geological relationships from large-scale mining datasets. Besides, many existing methods mainly focus on classification performance without offering proper interpretability concerning how geological attributes influence prediction outcomes. Therefore, there is a need for an effective deep learning approach that can learn hierarchical geological representations while also providing explainable decision analysis for reliable host rock recognition. To resolve these issues, this study introduces a Hierarchical Deep Representation Learning Model for Multi-Class Geological Host Rock Recognition (HDRL-MGHRR). The major contributions of this work are as follows:

- To develop a hybrid feature selection module using Mutual Information (MI), XGBoost feature importance, and LASSO methods for selecting important geological attributes.
- To design a hierarchical DL architecture integrating Variational Autoencoder (VAE), Hierarchical Capsule Network (HCapsNet), Memory-Augmented Neural Network (MANN), and Hierarchical Attention Layer for learning complex geological representations.
- To perform multi-class host rock classification using a Softmax classification layer for recognizing different geological host rock categories.
- To incorporate SHAP-based explainable geological AI analytics for geological feature interpretation, dependency analysis, and visualization of model predictions.
- To evaluate the presented HDRL-MGHRR method using the Mineral Ores Around the World dataset through different performance evaluation metrics.

II. Literature Review

In this section, a review of related works on machine learning and deep learning techniques for geological host rock and lithology classification is investigated. VISWANATH et al. [13] developed a DL methodology that incorporates Vision Transformers (ViT) with Fourier spectral filtering for RS lithology identification. To address a multi-class classification challenge, the system automates the procedure of detection and classification of several rock categories in RS imagery. Zhao et al. [14] designed an object detection and image recognition methodology to detect sedimentary, metamorphic, and igneous rocks. The author reviewed an enhanced YOLO11-based system by combining the Efficient Visual State Space (EVSS) component, improving the removal of fractures and texture by modeling long-range spatial dependencies. Kim and Youn [15] examined a new CNN with color histograms able to identify igneous rocks. General rock identification models applying DL depend only on CNNs to examine image pattern features. Antonini et al. [16] designed an RF-based prediction system that employs geochemical parameters to categorize ultramafic and mafic rocks interrupted by drill cores. Conversely, as methods become difficult, their interpretation can be significantly more complex. For interpreting the approach's performance, the study utilizes both local and global perspectives, integrating the SHAP algorithm. Xu et al. [17] investigated the unique benefits of CNNs in precisely recognizing underground rock formations and lithological structures, especially their robust feature extraction abilities. Furthermore, DL can effectively process large-scale data, thereby enhancing the precision and efficacy of classification.

Ma et al. [18] used fractal size to differentiate the geometric features of rock mass discontinuity and developed a data-based surrounding rock categorization (SRC) strategy combining ML methodologies. Critical parameters impacting the quality of the surrounding rock were studied and selected. Khajehzadeh et al. [19] proposed a novel ML algorithm for predicting RMDM utilizing the Q-system and rock mass rating (RMR) at the Khersan-2 dam site in southwestern Iran. Various effective ML approaches were used to evaluate RMDM. According to classification models, the site was rated as the best Q and RMR types. Veysi et al. [20] addressed an NMR-electrofacies architecture integrating Combinable Magnetic Resonance (CMR) logging with explainable ML to address these challenges. High-resolution CMR data were examined to measure pore structure features, permeability indicators, and fluid mobility parameters, with stimulated classification accomplished by optimizing an ML strategy integrating SHAP interpretability. The previous studies on rock classification models, including ML/DL techniques, key inputs, application areas, and main outcomes, are presented in Table I.

Many earlier studies used ML and DL approaches for rock and lithology classification. VISWANATH et al. [13] and Zhao et al. [14] mainly worked on image-based rock recognition, but they did not concentrate much on mining data with different geological relations. Kim and Youn [15] employed a CNN for rock classification, but the technique was limited in learning deeper geological relationships. Antonini et al. [16] utilized SHAP for interpretability, yet the work was mainly based on conventional models. Xu et al. [17], Ma et al. [18], and Khajehzadeh et al. [19] focused more on prediction accuracy and classification performance. However, feature selection, hierarchical deep learning, and explainable AI analysis were not combined in a single system. Because of this, there is still a need for a better model that can learn geological relationships effectively and also provide interpretable host rock classification results from mining datasets. Therefore, this study develops a model for learning geological relationships from mining data and provides host rock classification results.

TABLE I. SUMMARY OF ROCK CLASSIFICATION SYSTEMS

Authors & Years	ML/DL techniques	Key Inputs	Application area	Main outcomes
VISWANATH et al. [13]	ViT model	Lithology image patterns.	Lithology classification	Improved geological identification accuracy
Zhao et al. [14]	EVSS and YOLO11 approaches.	Visual spectral-spatial features.	Geological rock classification	mAP50 of 91.8%
Kim and Youn [15]	CNN and histogram algorithms.	Texture and color information.	Rock classification	Accuracy of 96.3%.
Antonini et al. [16]	ML and SHAP techniques.	Explainable geological features.	Igneous rock classification	F1 score of 96%.
Xu et al. [17]	CNN method	Radar signal features	Rock layer identification	Prediction results of 88%
Ma et al. [18]	Bayesian optimization, SVM, RF, and AdaBoost approaches.	Fractal characteristics.	Tunnel rock classification	Mi-F1 of 97.45%.
Khajehzadeh et al. [19]	ML models	Rock mass parameters.	Deformation modulus estimation	R2 of 0.99.
Veysi et al. [20]	NMR and ML methods.	Pore-type characteristics.	Carbonate reservoir classification	R2 of 0.89.

III. PROPOSED METHODOLOGY

Fig. 1 shows the overall workflow of the presented HDRL-MGHRR model for multi-class geological host rock recognition. Initially, the mining dataset is preprocessed, and important geological features are selected using feature selection techniques. Then, hierarchical geological representations are learned through the proposed DL architecture consisting of VAE, HCapsNet, a memory-augmented network, and an attention layer. Lastly, the learned representations are categorized into different host rock classes, and explainable geological AI analysis is carried out for the interpretation of the prediction results.

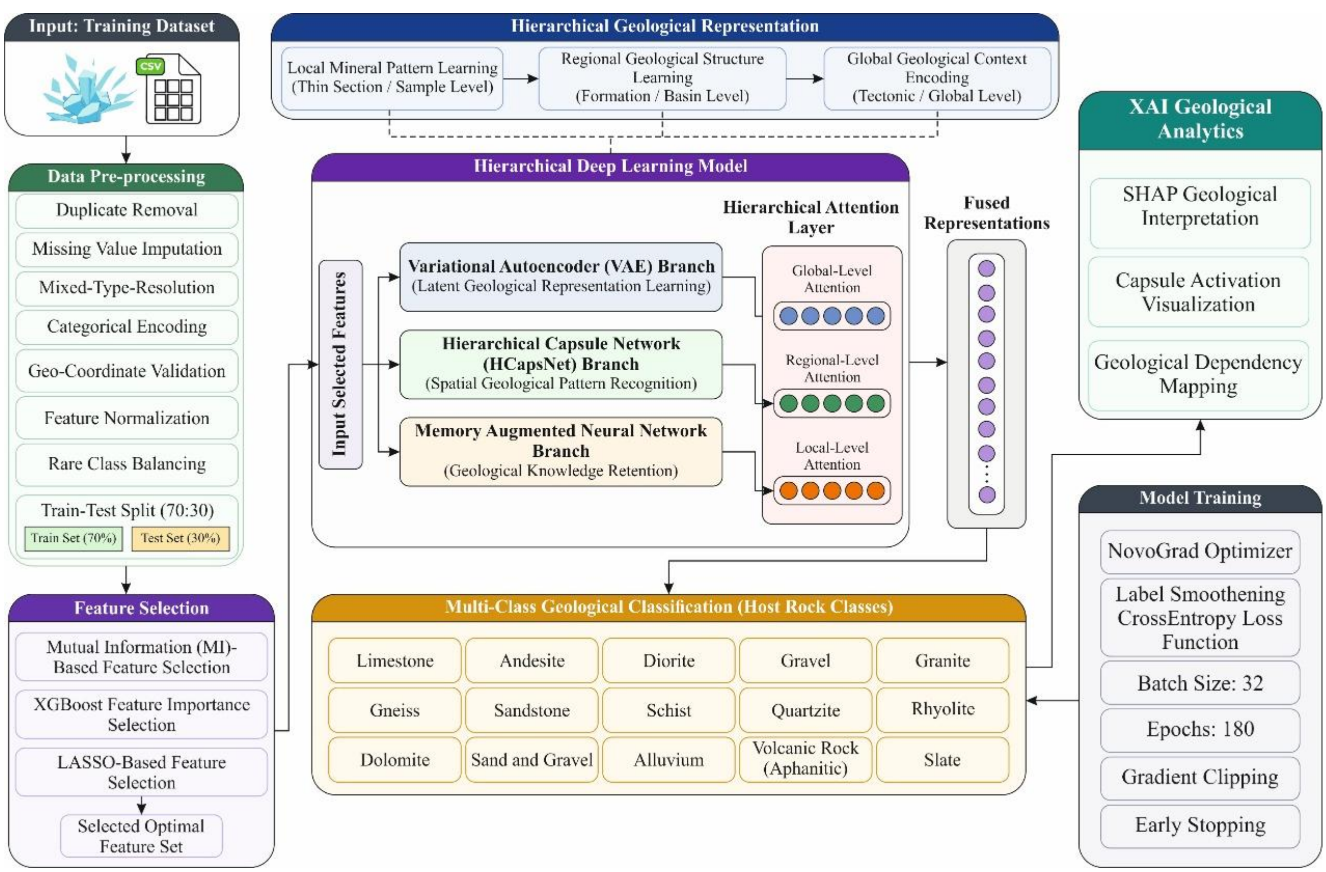

Fig. 1. Overall workflow of the presented approach.

A. Dataset Description

This section describes the dataset utilized for multi-class geological host rock classification. The performance assessment of the HDRL-MGHRR method by employing Mineral ores from all over the world [21]. The dataset encompasses information about different mineral ores discovered in various regions on a global scale. It contains 22 attributes, and it describes relevant geological information, locations, and mineral features; overall, 16 features were chosen for analysis. The dataset is valuable for exploratory data evaluation, ML, mineral classification, and mining-based research applications. The hrock_type distribution comprises a total of 37,687 instances with Limestone (6,931) as the most frequent rock type, followed by Andesite (3,382), Diorite (3,297), Gravel (3,265), and Granite (2,871). Other major rock categories include Gneiss (2,639), Sandstone (2,614), Schist (2,365), Quartzite (2,158), Rhyolite (1,569), Dolomite (1,560), Sand and Gravel (1,388), Alluvium (1,245), Volcanic Rock (1,206), and Slate (1,197), indicating a diverse geological composition across the dataset are represented in Fig. 2.

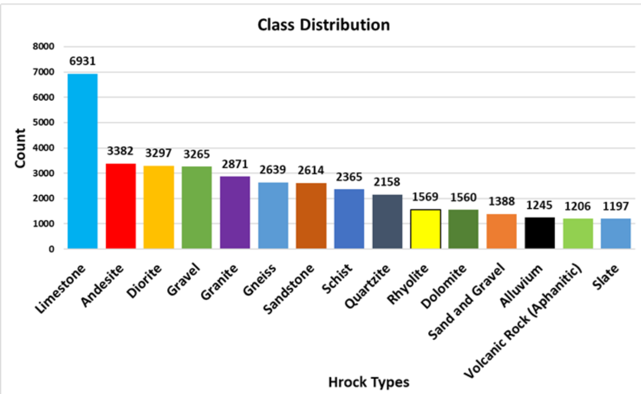

Fig. 2. Class distribution.

B. Data Preprocessing

This section describes the preprocessing steps applied to improve the quality of the mining dataset before model training. Data preprocessing is an important stage in the proposed multi-class geological host rock detection method [22]. The mining dataset contains duplicate records, missing values, categorical features, and inconsistent geo-coordinate information. The purpose of duplicate removal is to eradicate duplicate geological reports from the mining database. Missing values, including blank spaces, null values, and partial geological features, are managed utilizing appropriate imputation models. Mixed-type geological features signified in categorical and numerical formats are converted into a reliable representation. The categorical encoder procedure transforms geological data like mineral type, country, and deposit class into numerical representations appropriate for DL techniques.

Geo-coordinate validation is performed to validate longitude and latitude values and eliminate unreliable spatial geological reports. Feature normalization is used to scale geological features into the same numerical range to enhance model performance. The min-max normalization is expressed as:

$$X_{new} = \frac{X - \min(X)}{\max(X) - \min(X)} \quad (1)$$

In this Eq. (1), X_{new} implies the standardized geological feature data, X denotes the real geological feature data, $\min(X)$ and $\max(X)$ represent the minimal and maximal values of the attributes. Rare class balance is used to minimize geological host rock class imbalance. In conclusion, the database is split into a 70:30 train-test split ratio.

C. Feature Selection Strategy

This section offers the three-stage feature selection techniques utilized to identify the important geological attributes.

1) Mutual information-based feature selection: Mutual information (MI) is a measure in information theory that can be demonstrated as highly effective in variable selection due to its capability of detecting non-linear correlation amongst the parameters [23]. The information is derived from 2 random variables described by the MI between the two variables:

$$I(X;Y) = \sum_{x\in X}\sum_{y\in Y} p(x,y)\log\frac{p(x,y)}{p(x)p(y)} \quad (2)$$

In this work, MI is utilized to identify geological features having stronger dependency on host rock classes.

$$X_{s1} = \arg\max_{X_j} MI(X_j, Y), 1 \le j \le p \quad (3)$$

The subsequent feature is chosen by optimizing the MI between the particular feature subsets and the output:

$$X_{st} = \arg\max_{X_j} \ MI(\{X_{s1}, X_{s2}, \dots, X_{st}\}, Y) \quad (4)$$

2) XGBoost feature importance selection: The XGBoost feature importance method is used to identify geological features that highly influence host rock classification [24]. The importance scores are computed using gain, cover, and weight measures obtained from decision tree structures. Features with higher importance scores are selected for further geological representation learning.

3) LASSO-based feature selection: The LASSO regression is employed for choosing the most significant geological variables related to host rock prediction [25]. This method proficiently chooses important features by removing non-relevant ones by invalidating their coefficients. In the fundamental LASSO regression, the model coefficients decrease the residual sum of squares when combining the penalty factors:

$$\min\left(\sum_{i=1}^{n}(y_i - \hat{y}_i)^2 + \lambda\sum_{j=1}^{p}|\beta_j|\right) \quad (5)$$

$$Y = \beta_0 + \beta_1 X_1 + \beta_2 X_2 + \dots + \beta_p X_p + \varepsilon \quad (6)$$

The LASSO method removes less important geological features by shrinking insignificant coefficients toward zero, thereby improving feature selection efficiency and reducing overfitting.

D. Hierarchical Geological Representation

This section describes the process of learning multi-level geological representations from the selected features. The hierarchical geological representation learning phase is employed to acquire geological data with various ranges from the chosen mining features. The local mineral pattern learning concentrates on mineral relationships, ore-host interactions, and adjacent geological features present in the mining information. Regional geological structural learning gains geological dependencies and similarities among diverse deposit zones and mining regions. The global geological context encoding process learns the patterns of large-scale geological distribution and total host rock occurrence details that support increasing the performance of multi-class geological host rock classification. Moreover, the selected geological features are organized into three hierarchical levels based on their geological context. The local level represents sample-level mineralogical characteristics, the regional level denotes spatial and geological contextual information, and the global level represents broader geological characteristics. These three representations are processed by the presented model to acquire complementary geological patterns at different levels. The resulting local, regional, and global representations are subsequently integrated by the hierarchical attention mechanism and fused for final host rock classification.

E. Hierarchical Deep Learning Model

This section defines the proposed hierarchical deep learning method used for host rock recognition. The model integrates VAE, Capsule Network, Memory-Augmented Network, and Attention layer for multi-class lithology classification. However, the VAE, HCapsNet, and MANN representations are organized based on local, regional, and global geological contexts. The hierarchical attention mechanism assigns significance to the relevant representations at every level, and the resulting attention-weighted features are fused into a unified representation for final host rock classification. The overall architecture is demonstrated in Fig. 3.

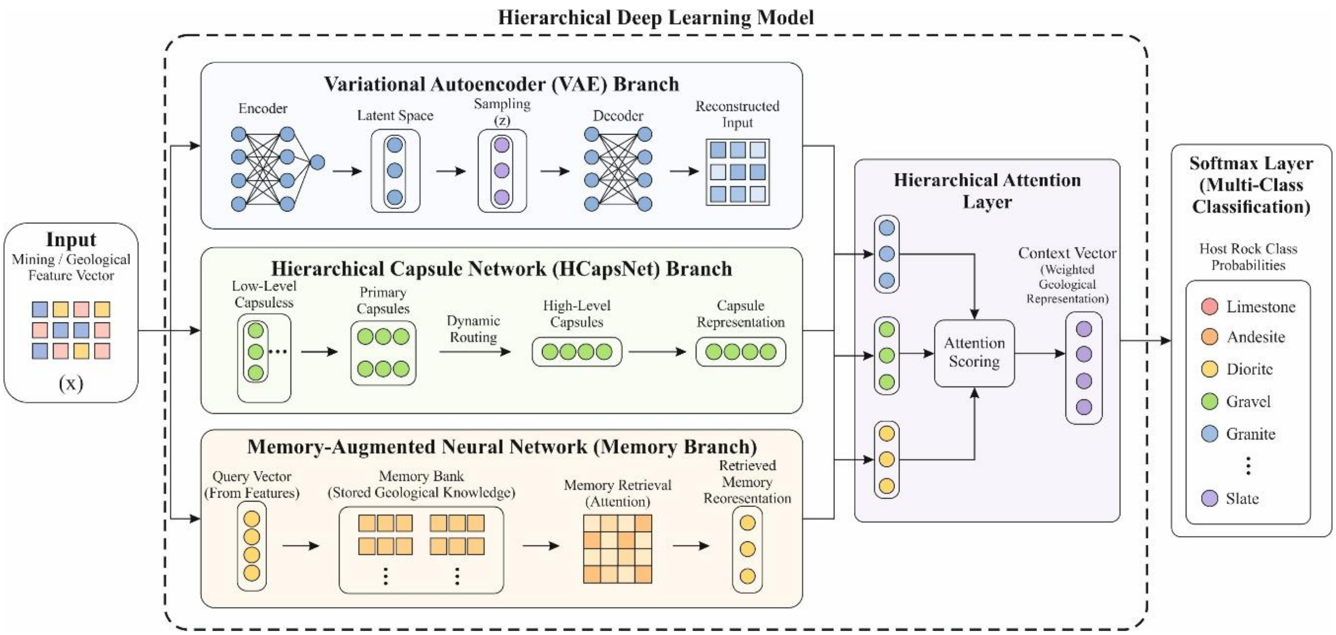

Fig. 3. Hierarchical deep learning architecture.

1) Variational autoencoder (VAE) branch: The VAE branch is utilized for latent geological representation learning [26]. Consider an input geological feature vector (x), the VAE encoder obtains the latent space using the Eq. (7), (8), and (9). Later, the parameters can be utilized to produce the latent variables (z). Furthermore, the VAE branch learns a compact latent representation of the selected geological features, capturing the underlying patterns while reducing redundant information. In conclusion, the VAE decoder applies the latent parameters to reconstruct the input vector of geological representation.

$$\mu = W_2 h + b_2 \tag{7}$$

$$\log var = W_3 h + b_3 \tag{8}$$

$$z = \mu + \epsilon \times e^{0.5 \times \log var} \tag{9}$$

Here, the term h refers to the output of the hidden layer (HL), the symbol μ and $\log var$ indicate latent space factors, the parameters $\{W_1, W_2, W_3, b1, b2, b3\}$ represent weights and biases, and the mathematical representation is $\epsilon \sim N(0,1)$.

The VAE branch is employed to learn latent geological representations from the chosen mining features for boosted performance of host rock classification.

2) Hierarchical capsule network (HCapsNet) branch: This section presents the HCapsNet branch used for spatial geological pattern learning. The capsule network is an advanced framework in the domain of DL developed to overcome the complexity of reducing spatial positional interactions in conventional NNs [27]. The main concept of CapsNet is the fundamental component, named the capsule. Every capsule is not only comprised of scalar values, but it also captures feature vectors that signify numerous features of individuals. Besides, the HCapsNet branch acquires hierarchical relationships between geological features through capsule-based representations, preserving dependencies among lower- and higher-level patterns. This strategy maintains the spatial hierarchical correlation between host rock structures, mineral relations, and geological features. This method allows the proposed model to recognize the mineral dependency patterns and geological formations more precisely, thus improving the capability of the network for spatial hierarchical and geological correlations.

$$v_j = \frac{\| s_j \|^2}{1+\| s_j \|^2} \frac{s_j}{\| s_j \|} \tag{10}$$

Now, the parameter s_j represents the capsule j's overall input vectors, and the term v_j indicates the capsule j's output vector.

The spatial hierarchical representation ability of CapsNets enhances the identification of intricate host rock structures and geological patterns by employing mining datasets.

3) Memory-augmented neural network branch: This section describes the memory-augmented branch used for retaining geological information. The memory-augmented neural network (MANN) is developed as the solution for processes that require long-range context and sequential coherence [28]. The memory networks are presented by permitting external memory storage and retrieval, thus enabling models to recall and refer to previous details applicable to the existing input. In geological host rock identification, the memory-augmented branch stores significant geological interpretation and mineral dependency data obtained from prior geological instances. The MANN branch stores and retrieves relevant geological patterns using an external memory mechanism, enabling contextual information to contribute to the final representation. Many traditional memory-based systems are dependent upon a huge memory bank that can be developed as computationally stronger and challenging to handle efficiently. The proposed technique employs the memory retrieval process to regain significant geological data for enriched host rock prediction, particularly. This methodology supports the model in retaining geological reliability and increasing the identification of intricate geological patterns by employing large-scale mining datasets.

The memory retrieval process can be denoted by:

$$m_t = Attention(q_t, M) \tag{11}$$

From this mathematical form, the term q_t characterizes the query vector, the parameter M indicates the memory bank, and m_t describes the recovered geological memory representation.

4) Hierarchical attention layer: This section explains the hierarchical attention layer leveraged for learning important geological dependencies. The approach transmits the encoded geological representation from the DL branches to the hierarchical attention layer to allocate an importance-based proportional score [29]. The hierarchical attention layer assigns different significance weights to the local, regional, and global geological representations. The local attention focuses on sample-level mineralogical characteristics, the regional attention emphasizes spatial and geological contextual information, and the global attention acquires broader geological patterns. The resulting attention-weighted representations are then combined to form a unified feature representation for host rock classification. The hidden representation (h_i) of the geological feature (f_i) can be entered into the feed-forward neural network (FFNN) to obtain an encoder representation:

$$\alpha_i = \frac{\exp(u_i^T u_w)}{\sum_j \exp(u_j^T u_w)} \tag{12}$$

$$s = \sum_i \alpha_i h_i \tag{13}$$

Here, the factor u_w represents the context vector, the symbol α_i denotes the attention score, the parameter u_i points to the encoder geological feature representation, and s indicates the final attention-based geological modeling. The hierarchical attention layer supports the proposed method, which concentrates on the most significant geological features, mineral interactions, and spatial dependencies that contribute to the multi-class host rock classification. This method increases the capacity of feature learning and improves the total prediction performance of the proposed HDRL-MGHRR framework.

F. Multi-Class Geological Classification Using Softmax Layer

This section presents the Softmax classification layer used for recognizing different host rock classes. The softmax function is a critical activation function utilized in multi-class geological host rock classifier tasks [30]. It captures a vector of raw scores attained from the proposed hierarchical DL techniques and converts them into a probability function through the host rock categorization. It is vital for interpreting the method outcome as the geological host rock categorization probabilities. In mathematics, for a vector of outcome scores $(z = [z_1, z_2, \ldots, z_k])$, the softmax function calculates the probability $(P(y = k))$ for host rock class (k) as explained in Eq. (14):

$$P(y = k) = \frac{e^{z_k}}{\sum_{j=1}^{K} e^{z_j}} \tag{14}$$

Here, $P(y = k)$ implies the probability of geographical host rock class k, $z_k$implies the outcome score for class k, K signifies the overall count of host rock categories, and e^{z_k} indicates the exponential outcome score for class k

The softmax layer transforms the trained geological representations into the final host rock predictive probabilities, such as Greenstone, Limestone, Schist, Slate, Granite, and Quartzite. The softmax function is differentiable, which is significant for the gradient-driven optimizer approach utilized in neural network training. It allows the proposed HDRL-MGHRR method to efficiently learn geological feature interactions and enhance multi-class host rock classification outcomes.

G. Explainable Geological AI Analytics

This section explains the explainable AI techniques used for the interpretation and analysis of geological predictions.

1) SHAP geological interpretation: The aim of interpretable machine learning (ML) in geological host rock classification is to comprehend how the proposed model creates predictions and to respond to questions about the relations among input and output host rock classes and geological features, and what features are most significant in driving the prediction [31].

2) SHAP-based geological feature attribution: An alternative local interpretation technique is the main idea of Shapley value in game theory that distributes contributions of features while they cooperatively accomplish the prediction outcome. Shapley values measure the influence of all the geological input features in the model that provide the host rock classification.

The Shapley value is determined for a feature X_j,

$$\phi_j = \sum_{S \subseteq N \setminus \{j\}} \frac{|S|!(p - |S| - 1)!}{p!} [f(S \cup \{j\}) - f(S)] \quad (15)$$

In this mathematical expression, the term p refers to the total counts of geological features, the factor S represents the feature subset, the parameter $f(S)$ indicates the model prediction with features in S, and the parameter $f(Xj)$ denotes the prediction with feature X_j. The interpretation is that the Shapley value signifies marginal contribution averaged over the entire feature integration.

3) Capsule activation visualization: Capsule activation visualization has been employed to comprehend the spatial geological pattern recognition learned through the Hierarchical Capsule Network (HCapsNet) framework. This outputs a capsule module that characterizes the hierarchical geological formations, like regional developments and local mineral formations. The activation capability specifies the significance of spatial geological correlation in the classification process.

4) Geological dependency mapping: Geological dependency mapping evaluates correlation among host rock classes, mineral deposits, and spatial coordinates. This visualization shows how geological developments are circulated over the regions. The SHAP values are spatially calculated to recognize the impacts of the geological field.

5) Attention visualization: The hierarchical attention layer allocates adaptive weights to geological features and latent representations. This attention visualization is recognized in the geological fields, and mineral amalgamation gives maximum for classifying the host rock.

The incorporation of SHAP-based interpretation, capsule activation visualization, geological dependency, and mapping attention visualization offers a wide-ranging explainability model for the proposed hierarchical DL method, thereby increasing the interpretability of geological host rock classification methods.

IV. Model Training Configuration

This section presents the training settings and parameter configurations used for the proposed model. NovoGrad optimization works by standardizing gradient updates at the parameter group level instead of the specific parameter level, which enables it to effectively handle the higher-dimensional parameter space of the hierarchical DL methods [32]. This group-by-group gradient normalization steadies the upgrades by balancing gradient scales, avoiding uneven upgrades in multi-class geological host rock recognition. Particularly, the 2nd moment estimation is calculated as:

$$v_t = \beta_2 v_{t-1} + (1 - \beta_2) \parallel g_t \parallel^2 \quad (16)$$

Here, v_t denotes the 2nd moment estimation at iteration t, β_2 implies the exponential decay rate, and g_t signifies the gradient at iteration t. The upgrade rule of the parameter is expressed as:

$$\theta_{t+1} = \theta_t - \eta \frac{m_t}{\sqrt{v_t} + \epsilon} + \lambda\theta_t \quad (17)$$

In this Eq. (17), θ_t signifies the parameter of the method at iteration t, m_t implies momentum-based 1st moment estimation, η indicates the learning rate, v_t denotes the 2nd moment estimation, ϵ represents a smaller constant for numerical stability, and λ implies the regularization parameter. Moreover, Label Smoothing Cross-Entropy loss is utilized to minimize overconfidence in predictions and enhance generalization outcomes in multi-class classification.

$$L = -\sum_{i=1}^{K} y_i^{LS} \log(p_i) \quad (18)$$

where, K= total classes, p_i= predicted probability for class i, and y_i^{LS}= label-smoothed target value for class i.

The proposed model is trained employing a batch size of 32 over 180 epochs. Gradient clipping is used to avoid exploding gradients and stabilize deep model training, whereas early stopping is used to prevent overfitting and improve the performance of the framework.

V. Experimental Results and Discussion

This section discusses the experimental results and performance analysis of the presented HDRL-MGHRR approach.

A. Performance Metrics

For assessing the performance of the presented model, several standard classification metrics are used, including accuracy, precision, recall, F1-score, and AUC score. In these equations, TP indicates true positives, TN denotes true negatives, FP points to false positives, and FN signifies false negatives.

Accuracy assesses the overall correctness of the model and is defined as:

$$\text{Accuracy} = \frac{TP + TN}{TP + TN + FP + FN} \tag{19}$$

Precision measures how many predicted positive samples are actually correct:

$$\text{Precision} = \frac{TP}{TP + FP} \tag{20}$$

Recall quantifies how many actual positive samples are properly recognized:

$$\text{Recall} = \frac{TP}{TP + FN} \tag{21}$$

F1-score is the harmonic mean of precision and recall and offers a balanced measure:

$$\text{F1-score} = \frac{2^{*}Recall^{*}Precision}{Recall + Precision} \tag{22}$$

AUC (Area Under the Curve) measures the system's capability for distinguishing between classes using the ROC curve:

$$AUC = \int_0^1 TPR\, d(FPR) \tag{23}$$

B. Result Analysis

Fig. 4 exemplifies the confusion matrix of the HDRL-MGHRR technique by comparing actual rock classes with predicted categories. The higher values on the diagonal specify strong classification accuracy, although the lower off-diagonal values indicate that only some of the instances can be incorrectly categorized into alternate rock types. Table II shows the parameter settings of the proposed methodology.

TABLE II. PARAMETER SETTING

Category	Parameter	Setting
Input	Input feature dimension	16
	Number of classes	15
VAE	Encoder architecture	16 → 64 → 32
	Latent-space dimension	32
	Decoder architecture	32 → 64 → 16
	Activation function	ReLU
HCapsNet	Capsule configuration	8 × 8
	Capsule dimension	8
	Routing iterations	3
	Capsule activation	Squashing
MANN	Memory size	128 × 64
	Memory retrieval	Cosine-similarity-based Top-4
	Query/feature dimension	64
Hierarchical Attention	Number of attention levels	3
	Attention hidden dimension	32
	Attention mechanism	Additive attention + Softmax
Feature Fusion	Fusion method	Attention-weighted fusion
	Fused feature dimension	64
Classifier	Classifier	Fully connected + Softmax
Regularization	Dropout	0.2
	Weight decay	1×10^{-4}
Initialization	Weight initialization	Kaiming/He
	Bias initialization	Zero
Training	Optimizer	NovoGrad
	Batch size	32
	Epochs	180
	Loss function	Label-Smoothed Cross-Entropy
	Label smoothing	0.1
	Gradient clipping	Max norm = 1.0
	Early stopping	Enabled

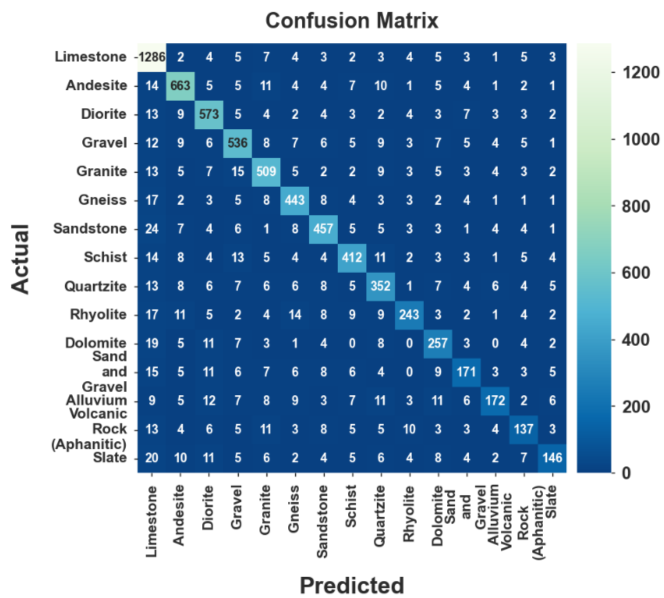

Fig. 4. Confusion matrix of the HDRL-MGHRR method.

Table III presents the multi-class rock recognition outcome of the HDRL-MGHRR approach with an 80:20 train-test split. The outcome implied that the HDRL-MGHRR method accurately classified the rock samples. The HDRL-MGHRR method achieved an average value $accu_y$ of 97.92% in TRAIP and $accu_y$ of 97.91% in TESTP, while the AUC_{score} of 89.10% for the TRAIP and AUC_{score} of 89.13% for the TRAIP, demonstrating the robustness and effectiveness of the proposed approach.

TABLE III. MULTI-CLASS ROCK RECOGNITION RESULTS OF THE HDRL-MGHRR METHOD WITH 80:20

Class Labels	$Accur_y$	$Preci_n$	$Recal_l$	$F1_{score}$	AUC_{score}
TRAIP (80%)					
Limestone	96.81	87.33	96.85	91.85	96.83
Andesite	97.84	86.15	89.87	87.97	94.24
Diorite	97.86	86.73	89.47	88.08	94.07
Gravel	97.62	85.68	87.43	86.55	93.02
Granite	97.80	84.01	87.61	85.77	93.12
Gneiss	98.07	87.46	84.96	86.19	92.01
Sandstone	97.88	84.23	85.20	84.71	92.01
Schist	98.18	85.63	84.99	85.31	92.02
Quartzite	97.62	79.20	79.01	79.10	88.88
Rhyolite	98.10	80.54	70.69	75.29	84.98
Dolomite	98.28	80.25	76.94	78.56	88.07
Sand and Gravel	98.00	78.36	64.48	70.75	81.89
Alluvium	98.36	80.33	65.40	72.10	82.43
Volcanic Rock (Aphanitic)	98.21	76.87	64.71	70.26	82.02
Slate	98.17	75.60	62.49	68.42	80.91
Average	**97.92**	**82.56**	**79.34**	**80.73**	**89.10**
TESTP (20%)					
Limestone	96.50	85.79	96.19	90.69	96.38
Andesite	97.82	88.05	89.96	88.99	94.32
Diorite	97.89	85.78	89.95	87.82	94.29
Gravel	97.61	85.21	86.04	85.62	92.35
Granite	97.78	85.12	86.71	85.91	92.72
Gneiss	98.18	85.52	87.72	86.61	93.33
Sandstone	98.01	86.06	85.74	85.90	92.34
Schist	98.06	86.37	83.57	84.95	91.32
Quartzite	97.60	78.75	80.37	79.55	89.51
Rhyolite	98.25	85.56	72.75	78.64	86.09
Dolomite	98.13	77.64	79.32	78.47	89.15
Sand and Gravel	98.14	76.68	66.02	70.95	82.65
Alluvium	98.22	83.09	63.47	71.97	81.49
Volcanic Rock (Aphanitic)	98.21	72.49	62.27	66.99	80.78
Slate	98.25	79.35	60.83	68.87	80.16
Average	**97.91**	**82.76**	**79.39**	**80.80**	**89.13**

Fig. 5 demonstrates the confusion matrix of the HDRL-MGHRR system by comparing actual rock types with predicted classes. The maximal values on the diagonal represent strong classification accuracy, even though the minimal off-diagonal values indicate that only a small number of samples were inaccurately categorized into other rock classes.

Table IV represents the multi-class rock recognition outcome of the HDRL-MGHRR method with a 70:30 train-test split. The experimental outcome values indicate that the HDRL-MGHRR system precisely categorized the rock instances. The HDRL-MGHRR technique accomplished an average value $accur_y$ of 97.38% in TRAIP and $accur_y$ of 97.31% in TESTP, and then the AUC_{score} of 86.39% for the TRAIP and AUC_{score} of 85.98% for the TRAIP, signifying the robustness and efficiency of the proposed model.

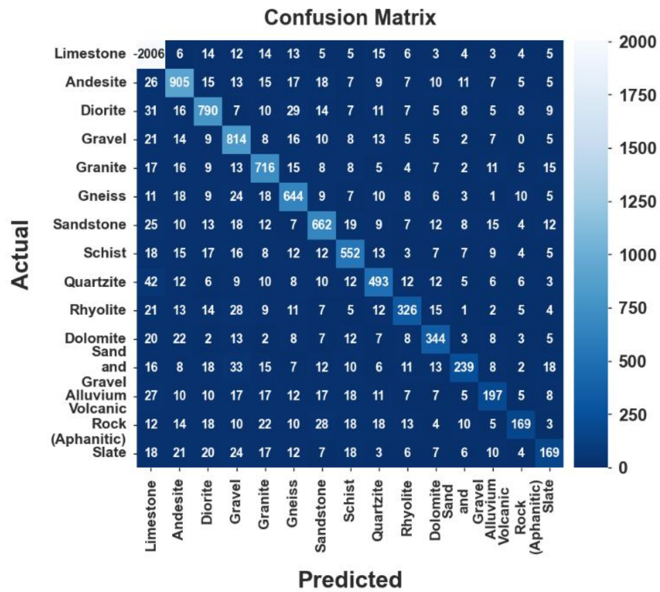

Fig. 5. Confusion matrix of the HDRL-MGHRR method.

TABLE IV. MULTI-CLASS ROCK RECOGNITION RESULT OF THE HDRL-MGHRR METHOD WITH 70:30

Class Labels	$Accur_y$	$Preci_n$	$Recal_l$	$F1_{score}$	AUC_{score}
TRAIP (70%)					
Limestone	96.60	87.35	95.16	91.09	96.04
Andesite	96.81	79.38	85.94	82.53	91.90
Diorite	96.94	82.08	83.76	82.91	90.99
Gravel	97.15	82.22	86.38	84.25	92.29
Granite	97.08	78.63	84.90	81.65	91.49
Gneiss	97.05	77.56	81.73	79.59	89.97
Sandstone	97.46	80.63	82.03	81.32	90.30
Schist	97.49	80.87	78.88	79.87	88.81
Quartzite	97.52	78.19	78.70	78.44	88.68
Rhyolite	97.68	74.44	67.24	70.66	83.12
Dolomite	97.87	75.55	72.17	73.82	85.58
Sand and gravel	97.67	73.01	58.44	64.91	78.80
Alluvium	97.70	68.24	57.81	62.59	78.44
Volcanic Rock (Aphanitic)	97.79	73.93	48.59	58.64	74.01
Slate	97.88	75.56	51.35	61.14	75.39
Average	**97.38**	**77.84**	**74.21**	**75.56**	**86.39**
TESTP (30%)					

Limestone	96.34	86.80	94.85	90.65	95.76
Andesite	96.82	82.27	84.58	83.41	91.34
Diorite	96.98	81.95	82.55	82.25	90.43
Gravel	96.82	77.45	86.87	81.89	92.29
Granite	97.24	80.18	84.14	82.11	91.22
Gneiss	97.21	78.44	82.25	80.30	90.28
Sandstone	97.04	80.15	79.47	79.81	88.95
Schist	97.35	78.19	79.08	78.63	88.82
Quartzite	97.39	77.64	76.32	76.97	87.49
Rhyolite	97.78	75.81	68.92	72.20	83.98
Dolomite	97.94	75.27	74.14	74.70	86.55
Sand and gravel	97.77	76.11	57.45	65.48	78.38
Alluvium	97.63	67.01	53.53	59.52	76.32
Volcanic Rock (Aphanitic)	97.79	72.22	47.74	57.48	73.57
Slate	97.57	62.36	49.42	55.14	74.24
Average	**97.31**	**76.79**	**73.42**	**74.70**	**85.98**

Table V shows the comparison outcome of the HDRL-MGHRR approach with existing methods using evaluation metrics, error rate, and execution time. The findings show that the HDRL-MGHRR method achieves better performance. The TS-FIS, AdaBoost, LogitBoost, RUSBoost, XGBoost, FT-Transformer, DCNv2, and TabNet approaches have lower outcomes. At the same time, the proposed HDRL-MGHRR system has achieved greater performance with $accur_y$ of 97.91%, $preci_n$ of 82.76%, recall of 79.39%, $F1_{score}$ of 80.80% and AUC of 89.13%. However, among the considered models, only FT-Transformer, DCNv2, and TabNet were reimplemented, while the remaining models were directly referred to from previously published papers [33].

TABLE V. COMPARATIVE RESULTS OF THE HDRL-MGHRR METHOD WITH OTHER APPROACHES

Algorithm	Accuracy	Precision	Recall	F1	AUC
TS-FIS	87.30	78.20	76.80	77.49	82.64
AdaBoost	89.20	80.40	78.90	79.64	84.18
LogitBoost	88.20	79.30	77.80	78.54	83.37
RUSBoost	85.30	74.60	72.90	73.74	80.91
XGBoost	88.20	79.80	78.10	78.94	83.76
FT-Transformer	92.60	81.20	78.60	79.88	86.21
DCNv2	91.80	80.60	77.90	79.22	85.73
TabNet	93.40	82.10	78.80	80.42	86.84
HDRL-MGHRR	**97.91**	**82.76**	**79.39**	**80.80**	**89.13**

An ablation study evaluates a model by removing or modifying its components to understand their individual contributions to performance. It helps identify the most important parts of the system and supports better model design and optimization.

TABLE VI. ABLATION STUDY OF THE HDRL-MGHRR METHOD WITH METRICS

Techniques	**Accuracy**	**Precision**	**F1-Score**
Without Feature Selection	91.84	69.72	67.85
MI Only	92.67	72.18	70.43
LASSO Only	92.91	72.84	71.16
XGBoost Feature Importance Only	93.14	73.56	71.82
VAE Only	93.58	75.21	73.14
HCapsNet Only	94.26	77.08	74.92
MANN Only	94.71	78.36	76.18
VAE + HCapsNet + MANN (without Hierarchical Attention)	96.38	81.47	79.96
HDRL-MGHRR (MI + XGBoost + LASSO + VAE + HCapsNet + MANN + Hierarchical Attention)	97.91	82.76	80.80

Table VI presents the ablation study of the HDRL-MGHRR approach with various metrics. The outcome implies that the Without Feature selection, MI only, XGBoost Feature Importance only, LASSO only, VAE only, HCapsNet only, MANN only, and VAE + HCapsNet + MANN (without Hierarchical Attention) approaches have gained minimal performance with various metrics, while the HDRL-MGHRR(MI + XGBoost + LASSO + VAE + HCapsNet + MANN + Hierarchical Attention) approach has obtained maximal performance with $accur_y$ of 97.91%, $preci_n$ of 82.76%, and $F1_{score}$ of 80.80%, indicating the effectiveness of the combined structure.

Fig. 6 presents the SHAP-based explanations for multi-class rock classification, illustrating both global and local feature contributions across different rock categories. The left panels show the global feature importance, indicating the overall contribution of variables such as ore type, location coordinates, and geological characteristics to the model predictions. The right panels provide local explanations, showing how individual feature values contribute positively or negatively to specific predictions. The SHAP analysis serves as the primary feature-level explanation, while the attention mechanism provides complementary insight into the relative focus assigned to the hierarchical representations. Together, these analyses provide a more transparent interpretation of the model's decision-making process.

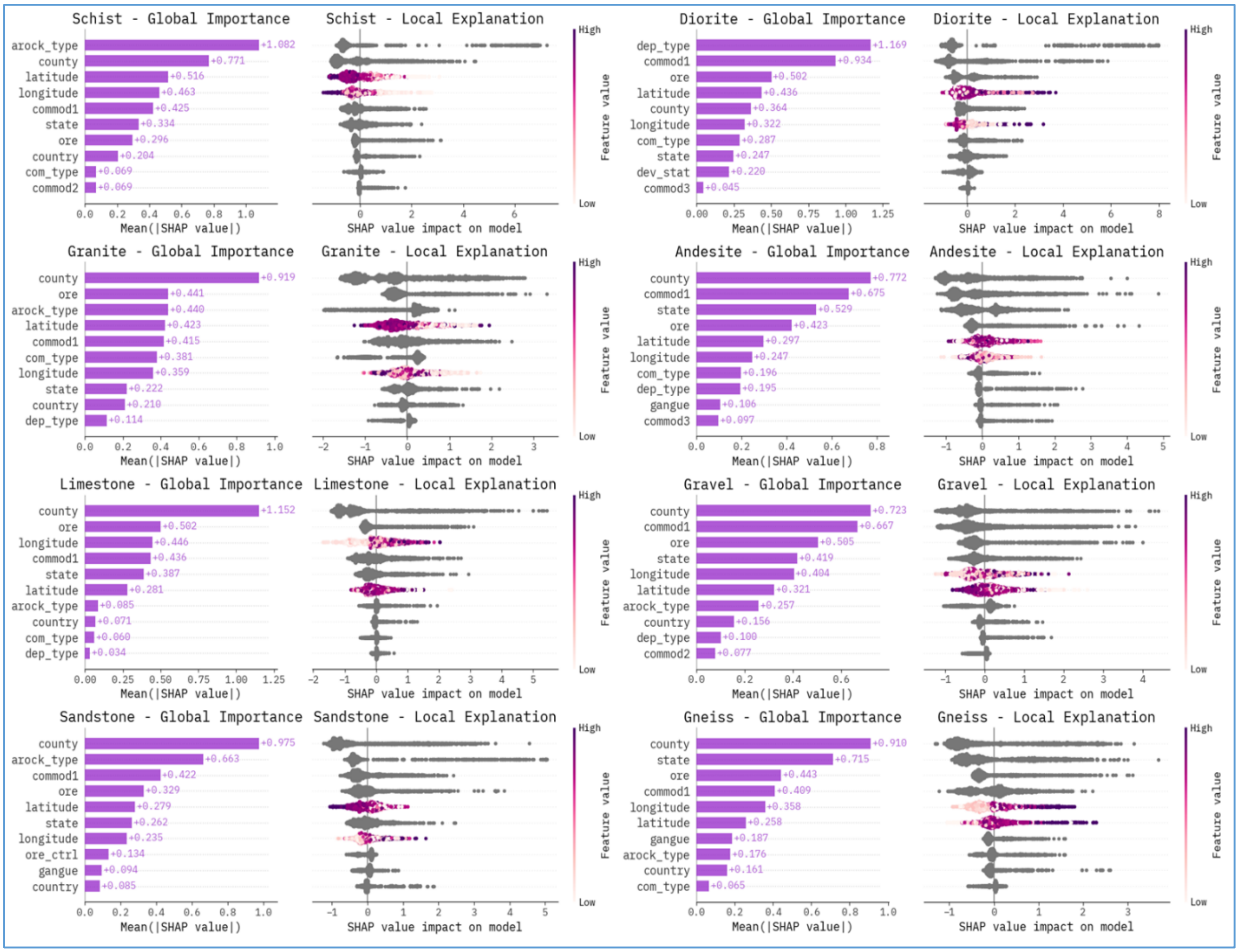

Fig. 6. SHAP values of the global and local explanations.

The experimental results illustrate that the presented HDRL-MGHRR architecture performs consistently over the 80:20 and 70:30 train–test splits, attaining approximately 97% accuracy with balanced precision, recall, and F1-score. To prevent data leakage, the dataset is first divided into training and testing partitions, with preprocessing parameters, class balancing, and feature-selection decisions based on Mutual Information, XGBoost, and LASSO learned exclusively from the training data, while the test set remained unseen until final evaluation. Class-wise results display higher performance for well-represented categories like Diorite, Andesite, and Limestone, while lower performance is observed for minority classes like Alluvium, Volcanic Rock, and Slate due to their limited representation and geological similarities. The difference between the overall accuracy of 97.91% and the class-average AUC of 89.13% is related to class imbalance, as accuracy could be influenced by better-represented classes, whereas AUC offers broader insight into class-wise discriminative ability. Class-wise metrics, confusion matrices, and MCC further aid the evaluation of per-class reliability. Comparative outcomes against Vision Transformer, ResNet variants, YOLO11, and DenseNet illustrate the proficiency and computational efficiency of HDRL-MGHRR. The ablation study further ensures the contributions of the feature-selection models and hierarchical components, illustrating that their incorporation offers efficient and computationally effective host rock classification.

VI. Conclusion and Future Work

This study has presented the HDRL-MGHRR model for multi-class geological host rock recognition using mining data analytics. The proposed model applied MI-based feature selection, XGBoost feature importance selection, and LASSO-based feature selection to select the most relevant geological attributes for host rock classification. A hierarchical DL approach consisting of a VAE, HCapsNet, Memory-Augmented Neural Network, and Hierarchical Attention Layer was developed to learn latent geological representations, spatial geological structures, and multi-level mineral dependencies from mining data. The learned geological representations were then categorized using a Softmax layer for recognizing multiple host rock classes. Furthermore, SHAP-based explainable geological AI analytics was used for geological feature interpretation and dependency analysis. This integration facilitated both global and local interpretation of predictions by identifying important geological features and mapping their contribution toward host rock classification through SHAP geological interpretation, capsule activation visualization, geological dependency mapping, and attention visualization. Experimental analysis on the Mineral Ores Around the World dataset showed the improved performance of the proposed HDRL-MGHRR approach in accomplishing interpretable multi-class geological host rock recognition.

Although the presented HDRL-MGHRR architecture illustrates efficient host rock classification on the evaluated dataset, the study is based on a static curated dataset and does not establish real-time deployment readiness. Temporal validation, geographically independent evaluation, field-level testing, robustness to measurement noise and missing data, and systematic operational latency assessment were not executed. Thus, the current outcomes primarily illustrate benchmark classification performance rather than validated real-world deployment capability. Future work will focus on validating HDRL-MGHRR using temporally independent and geographically diverse geological datasets, as well as real field measurements. Additional experiments will investigate robustness to sensor noise and missing attributes, and systematic latency and real-time deployment evaluations will be conducted to assess the practical suitability of the framework for geological monitoring and mineral exploration.

ACKNOWLEDGMENT

The authors extend their appreciation to Northern Border University, Saudi Arabia, for supporting this work through project number (NBU-CRP-2026-3030). This study is supported by funding from Prince Sattam bin Abdulaziz University, project number (PSAU/2026/R/1447).

DATA AVAILABILITY STATEMENT

The data that support the findings of this study are openly available in the Kaggle repository at https://www.kaggle.com/datasets/ramjasmaurya/mineral-ores-around-the-world [21].

CONFLICT OF INTERESTS

The authors declare no conflict of interest.

AUTHORS' CONTRIBUTION

The original contributions presented in the study are included in the article, further inquiries can be directed to the corresponding author.

REFERENCES

[1] Yang, W., Chen, Z., Zhao, H., Li, J., Chen, S., Shi, C., Li, Y., and Chen, D., 2026. EKTFD: Precise-guided empirical knowledge and time-frequency domain data joint-driven machine learning method for rock mass intelligent perception. Tunnelling and Underground Space Technology, 169, p.107303.

[2] Zeng, Y., Zhou, X., Yang, Y., Liu, X. and Yang, J., 2026. Application prospects of machine learning bridging rock/lithology identification and engineering rock mass characterization: A review. Tunnelling and Underground Space Technology, 174, p.107693.

[3] Luo, W., Xue, Y., Sun, Y., Zhang, W. and Wang, J., 2026. A knowledge-data dual-driven framework for predicting surrounding rock classification in TBM tunneling and generalization analysis. Tunnelling and Underground Space Technology, 170, p.107378.

[4] Li, Z., Zhang, Z., Xu, N., Gao, F. and Li, B., 2026. Characterizing Failure Mechanism of Soft and Hard Rocks: Implication from Acoustic Emission and Machine Learning. Rock Mechanics and Rock Engineering, pp.1-20.

[5] Chen, S., Hou, Y., Wang, R. and Zhao, X., 2026. Advance prediction of rock mass classification in tunneling using improved DS fusion and hybrid machine learning. Tunnelling and Underground Space Technology, 171, p.107453.

[6] Ma, J., Li, T., Yang, G., Dai, K., Ma, C., Tang, H., Wang, G., Wang, J., Xiao, B. and Meng, L., 2023. A real-time intelligent classification model using machine learning for tunnel surrounding rock and its application. *Georisk: Assessment and Management of Risk for Engineered Systems and Geohazards*, *17*(1), pp.148-168.

[7] Hasanipanah, M., Rouhani, M.M., Yin, X. and Rezaei, M., 2026. Prediction of Rock Blastability Index Using Rock Mechanics Properties and Advanced Machine Learning Techniques. Rock Mechanics and Rock Engineering, 59(4), pp.4471-4491.

[8] Markus, U.I., Ba, J., Abid, M., Faruwa, A.R. and Oli, I.C., 2026. Rock physics and machine learning for lithology identification and estimation of unconventional reservoir properties. Arabian Journal for Science and Engineering, 51(2), pp.1873-1894.

[9] Shi, D., Chen, X., Guo, Y. and Feng, L., 2026. In-Depth Understanding of the Compressive Failure Mechanism in Shotcrete–Rock Composites Using Non-destructive Techniques and Machine-Learning Algorithms. Rock Mechanics and Rock Engineering, pp.1-23.

[10] Liu, C.Y., Ku, C.Y. and Wu, T.Y., 2025. Advancing rock mass classification using machine learning approach. Bulletin of Engineering Geology and the Environment, 84(12), p.612.

[11] Nie, Y., Zhang, Q., Hou, L., Du, L., Zhao, X., Xue, Y., Lin, Z., Cao, X. and Wang, Z., 2025. TBM rock mass classification using XGBoost and Interpretable Machine learning. Advanced Engineering Informatics, 66, p.103459.

[12] Zhou, Z., Yu, J., Gao, J., Cai, X. and Wang, Z., 2025. Rapid rock mass classification framework using machine learning and semantic segmentation for underground mining. Engineering Applications of Artificial Intelligence, 159, p.111530.

[13] VISWANATH, M.G., KARTHIK, V.L.M., SUCHITHRA, S., FARHANA, K. and KUMAR, V.S., 2026. Deep Learning-Based Methods for Lithology Classification and Identificationin Remote Sensing Images. Research Digest on Engineering Management and Social Innovations, 2(4), pp.179-195.

[14] Zhao, F., Leng, X., Zhu, M., Luo, S. and Huang, J., 2026. Enhanced rock recognition via EVSS-integrated YOLO11: A deep learning approach for precise geological classification. PLoS One, 21(4), p.e0341862.

[15] Kim, D. and Youn, H., 2026. A Hybrid Deep Learning Approach Combining CNNs and Color Histograms for Improved Rock Classification. Rock Mechanics and Rock Engineering, 59(2), pp.2483-2503.

[16] Antonini, A.S., Tanzola, J., Asiain, L., Ferracutti, G.R., Castro, S.M., Bjerg, E.A. and Ganuza, M.L., 2024. Machine Learning model interpretability using SHAP values: Application to Igneous Rock Classification task. Applied Computing and Geosciences, 23, p.100178.

[17] Xu, H., Yan, J., Feng, G., Jia, Z. and Jing, P., 2024. Rock layer classification and identification in ground-penetrating radar via machine learning. Remote Sensing, 16(8), p.1310.

[18] Ma, J., Li, T., Shirani Faradonbeh, R., Sharifzadeh, M., Wang, J., Huang, Y., Ma, C., Peng, F. and Zhang, H., 2024. Data-driven approach for intelligent classification of tunnel surrounding rock using integrated fractal and machine learning methods. Fractal and Fractional, 8(12), p.677.

[19] Khajehzadeh, M., Keawsawasvong, S., Motahari, M.R. and Jamsawang, P., 2024. Effective machine-learning models for rock mass deformation modulus estimation based on rock mass classification systems. Engineered Science, 29, p.1120.

[20] Veysi, M., Kadkhodaie, A., Arian, M., Aleali, M., Maleki, Z. and Kianoush, P., 2025. Integrating NMR and machine learning for pore-type driven rock classification in the heterogeneous Asmari carbonate reservoirs. Scientific Reports.

[21] https://www.kaggle.com/datasets/ramjasmaurya/mineral-ores-around-the-world

[22] Beshah, Y.K., Abebe, S.L. and Melaku, H.M., 2024. Drift adaptive online DDoS attack detection framework for IoT system. Electronics, 13(6), p.1004.

[23] Riyanto, A., Kuswanto, H. and Prastyo, D.D., 2022. Mutual information-based variable selection on latent class cluster analysis. Symmetry, 14(5), p.908.

[24] Wang, W., Xiong, W., Wang, J., Tao, L., Li, S., Yi, Y., Zou, X. and Li, C., 2023. A user purchase behavior prediction method based on xgboost. Electronics, 12(9), p.2047.

[25] Heilemann, J., Klassert, C., Samaniego, L., Thober, S., Marx, A., Boeing, F., Klauer, B. and Gawel, E., 2024. Projecting impacts of extreme weather events on crop yields using LASSO regression. Weather and Climate Extremes, 46, p.100738.

[26] Zhang, F., Wei, Y., Liu, J., Wang, Y., Xi, W. and Pan, Y., 2022. Identification of autism spectrum disorder based on a novel feature selection method and variational autoencoder. Computers in Biology and Medicine, 148, p.105854.

[27] Yasenjiang, J., Xiao, Y., He, C., Lv, L. and Wang, W., 2024. Fault diagnosis of bearings with small sample size using improved capsule network and Siamese neural network. Sensors, 25(1), p.92.

[28] Umirzakova, S., Muksimova, S., Mardieva, S., Sultanov Baxtiyarovich, M. and Cho, Y.I., 2024. Mira-cap: Memory-integrated retrieval-augmented captioning for state-of-the-art image and video captioning. Sensors, 24(24), p.8013.

[29] Khan, S., Fazil, M., Sejwal, V.K., Alshara, M.A., Alotaibi, R.M., Kamal, A. and Baig, A.R., 2022. BiCHAT: BiLSTM with deep CNN and hierarchical attention for hate speech detection. Journal of King Saud University-Computer and Information Sciences, 34(7), pp.4335-4344.

[30] Alshaari, H. and Alqahtani, S., 2025. Deep-EFNet: An Optimized EfficientNetB0 Architecture With Dual Regularization for Scalable Multi-Class Brain Tumor Classification in MRI. IEEE Access.

[31] Li, Z., 2022. Extracting spatial effects from machine learning model using local interpretation method: An example of SHAP and XGBoost. Computers, Environment and Urban Systems, 96, p.101845.

[32] Wen, C., Qian, Y. and Huang, K., An Adaptive CPS Based Deep Evolving Fa-Gan Model to Address Urban Food Security and Socioeconomic Inequality in Smart City. Available at SSRN 5390944.

[33] Gholami Vijouyeh, A., Kadkhodaie, A., Siahcheshm, K., Asadi, A. and Hosseinzadeh, M., 2026. Integrated ore classification using stand-alone and hybridised machine learning algorithms. Scientific Reports, 16(1), p.14625.